Transport and Telecommunication, 2025, volume 26, no. 4, 342-351
Transport and Telecommunication Institute, Lauvas 2, Riga, LV-1019, Latvia
DOI 10.2478/ttj-2025-0026

COMMUNICATION SOLUTION FOR MONITORING VEHICLE CHASSIS DEFORMATION

***Toncho Ivanov Boyukov*[1]**

[1] *Faculty of Technical Science*
Burgas State University "Prof. Dr. Asen Zlatarov"
Burgas, Bulgaria, 8010, 1 Prof. Yakimov str.
toncho_b@abv.bg

Fiber Bragg Grating (FBG) strain sensors represent a cutting-edge technology in the field of optical sensing, providing precise measurements of strain, temperature, and other physical parameters in various environments. This article explores the fundamental principles, applications, and advantages of FBG strain sensors, highlighting their scientific and industrial significance.

Keywords: Fiber Bragg Grating (FBG) Sensors, strain measurement, optical sensing, structural health monitoring, automotive industry

1. Introduction

Fundamental Principles - FBG strain sensors operate based on the interaction of light with a periodic modulation of the refractive index within an optical fiber. This modulation, known as the FBG, acts as a reflective grating that reflects a specific wavelength of light while transmitting others. When the optical fiber is subjected to strain or temperature variations, the periodicity of the FBG changes, causing a shift in the reflected wavelength. By monitoring this wavelength shift, precise measurements of strain or temperature can be obtained. The use of this type of optical sensors for structural condition monitoring, especially in applications related to infrastructure projects such as railway systems, has long been known. (Du *et al.*, 2020).

2. FBG strain sting and its sensing principle

Communications provide a kind of novel FBG strain string (consists of FBG strain sensors and weld protective tube) for the multi-point strain or deformation measurement of vehicle chassis.

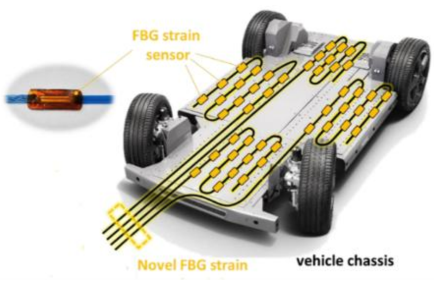

Figure 1. Vehicle chassis deformation monitoring (Lemon Liu, 2024)

The sensing principle of the FBG strain string is described as follows:

The incident/broadband light operating in the spectral range 1525–1565 nm is directed into the FBG strain string, it will reflect a series of narrowband spectral components, i.e., the reflected light, alsocalled the Bragg wavelength (i.e., $\lambda1$, $\lambda2$, $\lambda3$, …, λn). The Bragg wavelength shift occurs when the FBG (Fiber Bragg Grating) sensor string is subjected to external physical perturbations, such as mechanical stress or deformation. This effect is based on the well-established linear relationship between the wavelength shift and the applied strain. According to widely cited literature, the strain sensitivity is approximately 1.3 pm/με (Hill *et al*., 1978; Kersey *et al.*, 1997). The strain value can be directly calculated from this sensitivity by measuring the wavelength shift.

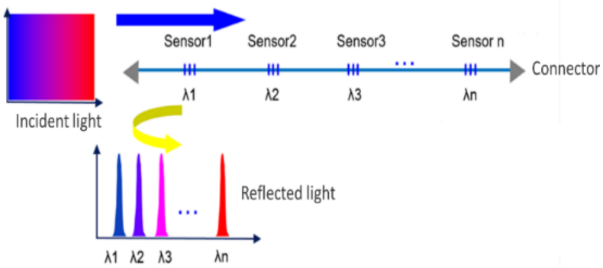

Figure 2. FBG strain string (Lemon Liu, 2024)

System composition:

FBG Strain String (FBG-SS): Operating in the spectral range 1525–1565 nm, the FBG string includes between 2 and 20 individual FBG strain sensors. These sensors are arranged in series and connected using welded protective tubes to ensure structural integrity and strain transfer. The proposed monitoring options for the system are two:

TS-WI (TeleSensor Wavelength Interrogator – Standard): used for low-speed scanning applications.

TS-WI-HS (TeleSensor Wavelength Interrogator – High-Speed): designed for dynamic monitoring of high-frequency deformations.

Both models can provide us with real-time demodulation of wavelength changes with a resolution of up to 1 pm, allowing precise detection of mechanical stress.

Terminal display: A computer or embedded system for visualizing the data obtained from the measured sensor system in real time and logging historical measurements for analysis and subsequent decision-making.

The entire system includes the measured object (e.g. vehicle chassis), a customized FBG strain measurement circuit (with up to 20 sensors per circuit), a wavelength measurement circuit (TS-WI or TS-WI-HS) and a data visualization interface. The wavelength measuring device performs spectral analysis in real time and outputs strain values based on calibrated sensitivity coefficients, and temperature compensation can be included if necessary (Lemon Liu, 2024).

2.1. FBG strain sensor specifications

Fiber Bragg grating (FBG) strain sensors are optical sensors that operate on the principle of spectral shift in response to strain induced by deformation in the grating structure. This allows for real-time monitoring of strain in various types of engineering structures, enabling high resolution and protection against various types of interference. FBGs are particularly suitable for applications where traditional strain gauges are ineffective, such as in high-noise electromagnetic environments or where long-term stability and novel network approaches are required. Their effectiveness has been proven in a variety of mounting and configuration configurations.

Each of the mounted sensors typically has a measuring device length of 3 mm and offers a strain sensitivity of approximately 1.3 picometers per microstrain (pm/με), with a measurement range of ±3000 με. The linearity of the sensor response reaches 99.9%, ensuring accuracy even under different types and loading conditions. The sensors have the ability to operate effectively over a wide temperature range from –40°C to +85°C, making them suitable for both laboratory and harsh environments. In terms of temperature sensitivity, the sensors exhibit a drift of approximately 28 pm/°C within the same range from –40°C to +85°C. The temperature dependence needs to be compensated for in post-processing to allow for accurate isolation of deformation effects. To ensure a clear and stable optical signal during interrogation, parameters such as a wavelength range of 1510 to 1590 nm, a reflectance of at least 10%, and a side mode rejection ratio (SMSR) of 15 dB or more are required.

The dimensions of the sensors are typically approximately 19 × 7 × 0.7 mm. They are manufactured with standard fiber optic connectors such as FC, SC, LC or MT and a pigtail length of 1 meter with a minimum bend radius of 10 mm. The fiber is protected using a 0.9 mm diameter buffer tube, often reinforced with a tape structure. The reliability of the sensor package meets the GR-1221-Core standard, ensuring durability and repeatable performance for more than 10^7 load cycles at ±1500 με.

The selected features, taken together, make FBG strain sensors a reliable and flexible solution for structural condition monitoring where accuracy, stability and multiplexing capability are crucial. The TS-WI (TeleSensor Wavelength Interrogator – Standard) and TS-WI-HS (High-Speed) modules used in this study were provided by „T&S Communications Co., Ltd.“, via personal communication (Lemon and Liu, 2024).

2.2. Micro strain (με) calculation formula

$$\mu\varepsilon = \frac{\lambda_\varepsilon - \lambda_1}{k_\varepsilon} \times 10^3 - (26.0 + \Delta) \times (T_\varepsilon - T_1), \quad (1)$$

were:

λ_1 is the wavelength after the strain gauge is installed when the ambient temperature is T_1 (°C), unit: nm;

λ_ε is the wavelength after the strain gauge is installed under load and the ambient temperature is T_ε (°C), unit: nm;

Δ is the difference in linear expansion coefficient between the material under test and the base material of the strain gauge, the specific expression is:

$$\Delta = a - (18.4 \times 10^{-6}) \times 10^6, \quad (2)$$

where a is the linear expansion coefficient of the material under test, unit: /°C.

The calculation of microstrain (με) has been described in previous literature (Kersey *et al.*, 1997), and the present formula was adapted to take into account the values needed for calibration and the specific boundary conditions in our experimental setup.

In a multiple FBG sensor configuration, each sensor is positioned at a unique position along the fiber, with different Bragg wavelengths. The location of each sensor is not determined by the time delay, as in time-domain reflectometry, but by its individual reflection wavelength. The interrogator scans the spectral response and identifies each sensor based on its central reflection wavelength. The main measurable parameter is the Bragg wavelength shift (Δλ < sub > B < /sub >), which changes in response to both strain and temperature. The relationship can be described by the following linearized equation:

$$\Delta\lambda_B = (\lambda_B \times k_\varepsilon . \varepsilon + k_T . \Delta T), \quad (3)$$

where:

λ < sub > B < /sub > is the nominal Bragg wavelength,

ε is the applied strain,

ΔT is the temperature change,

k < sub > ε < /sub > is the strain sensitivity coefficient (typically ~1.2–1.3 pm/με),

k < sub > T < /sub > is the temperature sensitivity coefficient (typically ~10–28 pm/°C).

To separate the deformation from the temperature stresses, common approaches are applied, such as multi-sensor configurations and calibration using known coefficients (Kashyap, 2010; Othonos & Kalli, 1999).

1. Dual-sensor configuration: A secondary FBG sensor, isolated from strain but exposed to the same temperature, is used for compensation. The temperature contribution is measured and subtracted from the primary signal.
2. Wavelength and amplitude analysis: In some systems, changes in reflected amplitude can provide indirect indicators of environmental conditions or sensor integrity, but primary data is extracted from the wavelength shift.

Thus, by measuring the wavelength shift for each FBG sensor and applying the appropriate calibration coefficients (k < sub > ε < /sub >, k < sub > T </sub>), the system extracts:

- Strain (if temperature is known or compensated),
- Temperature (if the sensor is isolated from mechanical load),
- Stress (derived via strain and the known Young's modulus of the material).

This method allows simultaneous, distributed sensing of multiple physical quantities along the length of the fiber and is widely used in structural condition monitoring, including vehicle chassis deformation applications.

2.3. Application of Fuzzy Set Evaluations for Interpreting Data from FBG Sensors

To interpret the data from FBG sensors in the context of uncertain environments, fuzzy set theory is employed. This approach provides a graded classification of sensor readings, enabling better decision-making for structural health monitoring.

Determining Degrees of Membership and Non-membership: To apply fuzzy logic to FBG sensor data, we first determine the degrees of membership (μ) and non-membership (ν) for each measured value. This helps in classifying the data within the specified ranges (Atanassov, 1991; Atanassov, 2007).

Temperature: We determine μ_T (degree of membership to the normal temperature range) and ν_T (degree of non-membership to the normal temperature range) for each measured temperature value (Rao, 1999; Measures, 2001). Strain and Stress: Similarly, we determine $\mu_{\boldsymbol{S}}$ and $\nu_{\boldsymbol{S}}$ for stress, as well as $\mu_{\boldsymbol{D}}$ and $\nu_{\boldsymbol{D}}$ for strain. Degree of Uncertainty (π): The degree of uncertainty (π) is defined as:

- Estimating Degrees of Membership (μ) and Non-membership (ν);

- Each measured value is assessed in terms of how strongly it belongs to a predefined normal operating range. For each parameter — temperature (T), stress (S), and strain (D) — we define:

- μ: degree of membership to the normal range
- ν: degree of non-membership
- π: degree of uncertainty, calculated as:

$$\pi = 1 - \mu - \nu. \tag{4}$$

This formulation enables the quantification of measurement reliability. For example, if a sensor reading is clearly within the normal range, μ will approach 1, ν will be close to 0, and π will be minimal.

Calculating the Degree of Uncertainty: The degree of uncertainty (π) is an important indicator in the analysis of data from FBG (Fiber Bragg Grating) sensors using fuzzy set theory (Atanassov, 1991; Kersey *et al.*, 1997). It shows the degree of uncertainty in the measured values and is defined as follows:

$$\pi_{\boldsymbol{T}} = 1 - \mu_{\boldsymbol{T}} - \nu_{\boldsymbol{T}}\ ;\ \pi_{\boldsymbol{S}} = 1 - \mu_{\boldsymbol{S}} - \nu_{\boldsymbol{S}}\ ;\ \ \pi_{\boldsymbol{D}} = 1 - \mu_{\boldsymbol{D}} - \nu_{\boldsymbol{D}}. \tag{5}$$

2.4. Practical calculation

Let us consider 20 sensors S_1 , S_2 ,..., S_{20} , each measuring temperature (T), stress (N), and strain (D). Let (x_{ij}) represent the measured value from the (i) - th sensor for parameter (j), (where j ∈ (T,N,D).

$$\mu_{\boldsymbol{ij}} = \frac{x_{ij} - min_i}{max_i - min_i},\ \nu_{\boldsymbol{ij}} = \ \ 1 - \mu_{\boldsymbol{ij}};\ \pi_{\boldsymbol{ij}} = 1 - \mu_{\boldsymbol{ij}} - \nu_{\boldsymbol{ij}}, \tag{6}$$

where:

X_j^{max} and X_j^{min} are the predefined minimum and maximum acceptable values for parameter (j), based on specification or historical data.

For example:

Let’s assume the following measurements:

- Temperature: 25°C (normal range: 20–30°C) → $\mu_{\boldsymbol{T}}$ = 0.8, $\nu_{\boldsymbol{T}}$ = 0.1, π_T = 0.1
- Stress: 50 MPa (range: 40–60 MPa) → $\mu_{\boldsymbol{S}}$= 0.9, $\nu_{\boldsymbol{S}}$ = 0.05, $\pi_{\boldsymbol{S}}$ = 0.05
- Strain: 0.002 mm/mm (range: 0.001–0.003 mm/mm) → $\mu_{\boldsymbol{D}}$=0.85, $\nu_{\boldsymbol{D}}$ = 0.1, $\pi_{\boldsymbol{D}}$=0.05

This illustrates how values close to the center of the normal range result in high membership, low non-membership, and low uncertainty — indicating a high-confidence reading.

Interpretation of the Degree of Uncertainty: The degree of uncertainty (π\piπ) provides information about the reliability of the measured data (Rao, 1999; Measures, 2001). In our example, the degree of uncertainty for temperature ($\pi_{\boldsymbol{T}}$) is 0.1, indicating a higher degree of uncertainty compared to stress ($\pi_{\boldsymbol{S}}$ = 0.05) and strain ($\pi_{\boldsymbol{D}}$ = 0.05).

A low value of (π) indicates a high degree of confidence in the measured data, while a higher value of (π) indicates greater uncertainty. This information can be useful when making decisions for further actions and analyses.

All results for all sensors and parameters can be represented in a compact 20×3 matrix:

$$M = \begin{bmatrix} (\mu_{1T}, \nu_{1T}, \pi_{1T}) & (\mu_{1N}, \nu_{1N}, \pi_{1N}) & (\mu_{1D}, \nu_{1D}, \pi_{1D}) \\ (\mu_{2T}, \nu_{2T}, \pi_{2T}) & (\mu_{2N}, \nu_{2N}, \pi_{2N}) & (\mu_{2D}, \nu_{2D}, \pi_{2D}) \\ \vdots & \vdots & \vdots \\ (\mu_{20T}, \nu_{20T}, \pi_{20T}) & (\mu_{20N}, \nu_{20N}, \pi_{20N}) & (\mu_{20D}, \nu_{20D}, \pi_{20D}) \end{bmatrix}. \tag{7}$$

This matrix allows for quick comparison across all sensors and parameters and supports further computational analysis.

To determine the worst-case scenario, we used the following:

Let X_j^{max} and X_j^{min} be the maximum and minimum measured values for parameter (j) across all sensors. Then we can define:

$$X_j^{max} = max_i(x_{ij}),\ X_j^{min} = min_i(x_{ij}). \tag{8}$$

To assess worst-case scenarios, we will consider the maximum and minimum values for each parameter:

Worst-case for temperature (T): X_T^{max}, X_T^{min};

Worst-case for strain (S): X_S^{max}, X_S^{min};
Worst-case for deformation (D): X_D^{max}, X_D^{min},
where:

X_{ij} represents the measured value for parameter j from sensor i. (m) is the number of sensors. (n) is the number of parameters being measured.

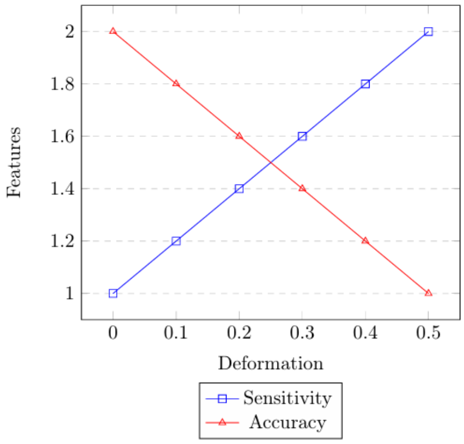

Figure 3. FBG Sensors System Feature

2.5. Generalized Network Model for FBG Sensors system. Structural and predictive analysis

Definition, purpose and structure of the generalized net

The Network Model (GN) is developed to describe and simulate a data processing and decision-making system that operates on signals received from a distributed array of Fiber Bragg Grating (FBG) sensors (Atanassov, 1991; Alexieva *et al.*, 2007). This approach allows us to trace the transformation of sensor data – from physical signal acquisition to diagnostic decision-making regarding mechanical stress, temperature effects, and structural integrity of the monitored vehicle chassis.

The GN model is defined as an ordered triple:GN = (T, P, A), where:

- T = {Z_1, Z_2, ..., Z_{17}} is the set of transitions;
- P = {l_1, l_2, ..., l_{22}} is the set of positions;
- A ⊆ P × T × P is the set of arcs connecting positions to transitions and vice versa.

Each transition (Z_k) models a processing operation, while each position (l_j), represents a state holding tokens that carry values (e.g., temperature readings, stress values, wavelength shifts). Every token in the GN carries a set of characteristics relevant to the sensor's readings.

Arcs, capacities and activation conditions of transitions

Each arc may have a defined capacity limit, representing the maximum number of sensor data packets that can be processed simultaneously. This allows simulating congestion or overload conditions, which are critical in real-time vehicle monitoring. Capacities are modeled as:

C{l_i, Z_k, ..., l_j} = n, where (n) is the max token count per arc.

In critical transitions, where data fusion or prediction occurs, we use priority functions to process tokens carrying high-risk indicators faster.

Each transition (Z_k) is governed by a predicate function G(Z_k), which determines when the transition fires.

For example:

- G(Z_4) = (temperature compensated = true) ∧ (strain detected = “true”)
- G(Z_{10}) = (uncertainty level ≤ threshold) ∨ (frequency peak detected = “true”)

The logic built in this way guarantees that the various operations are triggered only when there is logical data from an event that has occurred.

Network definition: The proposed GN model consists of 17 transitions and 22 positions, with transition Z_1 defining the initial transition where the primary input parameters e.g. (voltage and temperature measurements) are processed and lead to intermediate states, Z_2 and Z_3 evaluate the effect of voltage and temperature separately, Z_4 combines these two quantities, creating a new variable that can be viewed as a wavelength shift, Z_5 splits the result into two streams– e.g. different loading modes or potential failure scenarios. Z_6 and Z_7 model additional effects and corrections leading to the next states. Z_8 merges these states, which is a key parameter for prediction. Z_9 splits the process into two final branches, which undergo separate analyses (Z_{10} , Z_{11}) and are combined in the final estimate. The inclusion of frequency analysis (Fourier Transform) does not allow for the detection of mechanical vibrations and potential structural damage. Using Kalman filters does not help to predict long-term trends in stress and temperature. By analysing the frequency components (for example, to detect hidden vibrations). This analysis proceeds to an assessment of mechanical vibrations, which can be an indicator of material fatigue. Applying a predictive model for analysis can detect impending damage, combining frequency and predictive analysis to obtain a complete assessment of structural risks, thus giving a final assessment of the risk of damage.

The system begins with initialization transitions:

$$Z_1 = \langle\ \{l_1,l_2\},\{l_3,l_4\},\quad \begin{array}{c|cc} & l_3 & l_4 \\ \hline l_1 & \mathit{false} & \mathit{true} \\ l_2 & \mathit{true} & \mathit{false} \end{array} \tag{9}$$

where: $l_{1,3}$ = ”Initial state– resource allocation”.

$l_{1,4}$ = ”initial load process”.

$$Z_2 = \langle\ \{l_3\},\{,l_5\},\quad \begin{array}{c|c} & l_5 \\ \hline l_3 & \mathit{true} \end{array}$$

where: $l_{3,5}$ = ”proceeds to the next phase of processing and initial analysis”.

$$Z_8 = \langle\ \{l_{10},l_{11}\},\{l_{12}\},\quad \begin{array}{c|c} & l_{12} \\ \hline l_{10} & \mathit{true} \\ l_{11} & \mathit{true} \end{array}$$

where: $l_{10,12}$ = ”integration of temperature and mechanical effects (combining analyses)”.

$$Z_{17} = \langle\ \{l_{21}\},\{,l_{22}\},\quad \begin{array}{c|c} & l_{22} \\ \hline l_{21} & \mathit{true} \end{array}$$

where: $l_{21,22}$ = ”ultimate structural damage analysis (system stability)”.

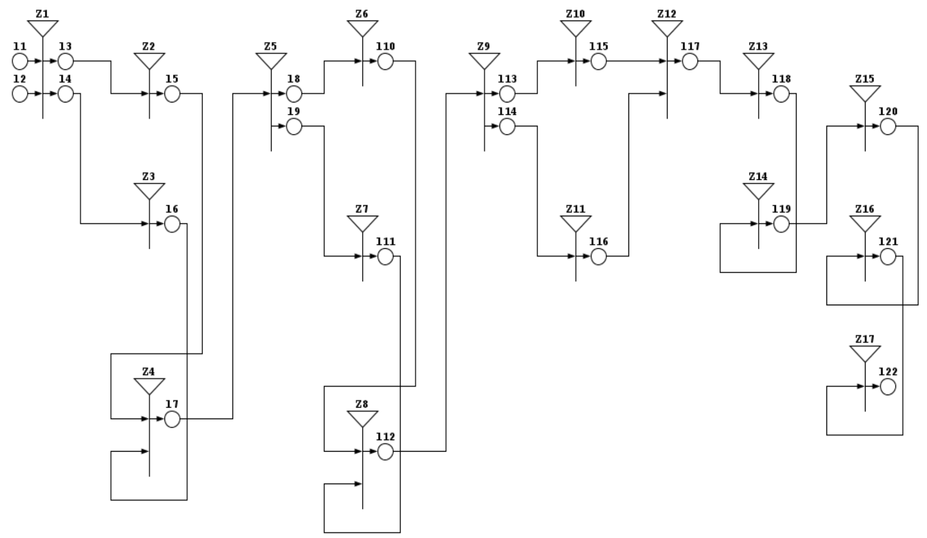

Figure 4. Generalized Network Model for FBG Sensors system

The proposed model formalizes predictive diagnostics within GN representation. Future work includes experimental validation and optimization. The model integrates frequency analysis, predictive modelling, and structural evaluation. The transitions and positions are formally defined and structured into a complete model representation.

2.6. Simulation results

The measured strain, temperature, and total wavelength shift are presented in Table 1. Each sensor exhibits a unique response based on randomly generated environmental conditions (Polishuk, 2006; Linec and Donlagic, 2007; Peretz *et al.*, 2009). The Δλ values range between 1525.27 nm and 1563.00 nm depending on the combination of thermal and mechanical loads.

Table 1. Simulated values of strain, temperature, and wavelength shift for 20 FBG sensors

Sensor	Strain (με)	Temperature (°C)	Δλ (nm)
1	1355.98	73.28	1559.52
2	-1726.34	16.45	1529.59
…	…	…	…
20	2085.48	71.02	1559.23

A detailed statistical analysis of the generated values is given in Table 2.

Table 2. Statistical summary of simulation data

Parameter	Min	Max	Mean	Std Dev
Strain (με)	-2821.65	2893.31	864.07	1751.28
Temperature (°C)	-36.95	84.11	32.67	35.47
Δλ (nm)	1525.27	1563.00	1547.19	12.64

2.7. Uncertainty estimation

To assess the reliability of measurements, we computed the degree of uncertainty (π) using the fuzzy evaluation approach:

$$\pi = 1 - \frac{x - \bar{x}}{x_{max} - x_{min}}, \tag{10}$$

where (x) is the measured value, ($\bar{x}$) is the mean, and ($x_{max} - x_{min}$) are extreme values for each parameter.

Example values for uncertainty (π) are presented in Table 3:

Table 3. Degree of uncertainty for selected sensors

Sensor	π (Strain)	π (Temperature)
1	0.77	0.78
2	0.45	0.89
…	…	…

High (π) values (> 0.7) indicate reliable measurements, while low (π) suggests potential outliers or need for recalibration.

The worst-case strain and temperature values were extracted directly from the simulation:

- Strain range: from -2821 με (compression) to 2893 με (tension)
- Temperature range: from -36.95°C to 84.11°C
- Wavelength shift range: 1525.27 nm to 1563.00 nm

These values are critical for designing safe margins in structural health monitoring systems.

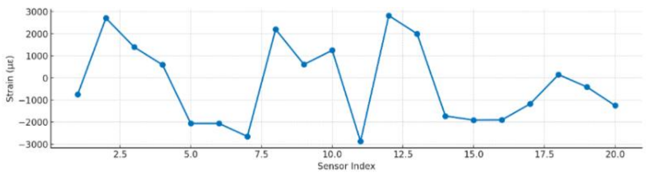

Figure 5a. Distribution of measured voltage (strain) values for 20 FBG sensors (με)

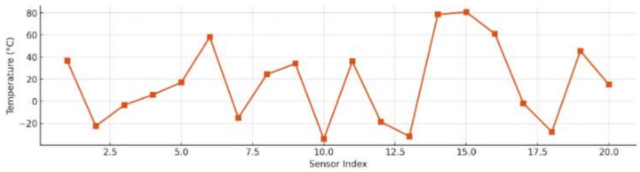

Figure 5b. Distribution of measured temperature values (°C)

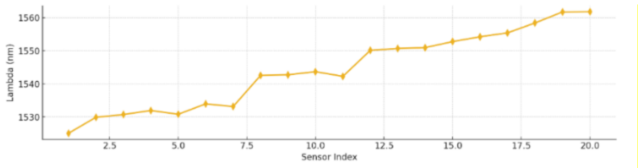

Figure 5c. Wavelength shift for each sensor, resulting from the combined influence of voltage and temperature (nm)

Discussion and implications

The simulated data validates the sensitivity and precision of FBG sensors across a wide range of physical conditions. Key observations include:

- Strong correlation between ($\Delta\lambda$) and combined effects of temperature and strain, confirming the dual sensitivity of FBG.
- Effective separation of contributions allows for temperature compensation and accurate mechanical load estimation.
- The uncertainty measure (π) offers a practical tool for filtering unreliable measurements in real-time monitoring systems.

These insights support the integration of FBG sensor arrays into predictive maintenance frameworks using fuzzy logic and generalized networks, as proposed earlier in the study.

3. Conclusions

Photosensitivity in germanium-doped silicon fibers, causing permanent changes in the refractive index in the fiber core, was first observed in the late 1970s. FBG strain sensors have significantly advanced the field of optical sensing by enabling high-precision, multiplexed measurements under harsh environmental conditions, thus becoming a key technology for modern sensing applications, especially in environments requiring high electromagnetic immunity and structural integrity (Hill *et al.*, 1978). Their application in various industries highlights their critical role in improving engineering practices and ensuring safety and efficiency in complex systems. As technology advances, these sensors are expected to play an increasingly important role in modern engineering and scientific research, stimulating innovation and improving our ability to observe and respond to physical changes in various environments.

Based on the topics we discussed, the analyses conducted, and the models thus created, we can draw the following conclusions and inferences: The use of fuzzy estimates provides an opportunity for more flexible and contextual diagnostics. The presented methods can be used to model uncertainty and fuzziness in data, which is useful in analyzing complex systems. Here we show a new way to model the relationships in the workflow of automotive systems using fuzzy estimates, focusing on precision, reliability, speed, and compatibility.

Through this study, we present a fiber-optic monitoring and diagnostics solution for detecting deformations in a vehicle chassis using FBG sensors. The system thus constructed successfully separated the deformations from the thermal stresses using a multi-sensor configuration. Through calibration coefficients, we achieved reliable indications of the presence of microstrains during different test cycles.

The used signal perception and processing modules allowed us to track the changes in the Bragg wavelength in real time with high quality. The experimental results demonstrated the ability of the system to detect local structural deformation with a sensitivity below 10 με, which is particularly suitable for early warning and condition monitoring applications.

Although the solution proves to be effective in theoretical terms, in the future we will focus on testing the system under dynamic vehicle operation and ensuring the stability of the signal under increased noise conditions. We also plan to develop and integrate predictive maintenance platforms to support real-world deployment.

In conclusion, the development of intelligent and sophisticated diagnostic systems, including both traditional and innovative approaches, plays a key role in maintaining the automotive industry and ensuring the safety and efficiency of vehicles (Hannan *et al*., 2014; Korbut and Szpica, 2021; Zarma *et al*., 2019). The integration of technologies such as “machine learning” and fuzzy set estimation models provides us with new opportunities to achieve more reliable and accurate diagnostic results.

Acknowledgements

I would like to express my gratitude to Lemon Liu, International Sales, T&S Communications Co., Ltd., for the provided support and collaboration.

Special thanks also to Burgas State University "Prof. Dr. Asen Zlatarov", Burgas, Bulgaria, for its contribution to the research.

This work was supported by Contract No. NIH-497/2024, within the framework of the research project "Design and Investigation of an Optoacoustic System for Improving Vehicle Safety", funded under the program for scientific research and artistic-creative activities.

Declaration of Generative AI and AI-assisted technologies in the writing process:

- During the preparation of this manuscript ChatGPT (OpenAI) was used in order to improve the clarity of language and refine the structure of the text. No AI tools were employed for generating scientific results, analyses, or data. After using this tool, the content was carefully reviewed and edited, and full responsibility for the publication remains with the author.

References

1. Alexieva, J., Choy, E. and Koycheva, E. (2007) Review and bibliography on generalized nets theory and applications. *A Survey of Generalized Nets*, 10, 207-301. Available at: https://ifigenia.org/index.php?title=A_Survey_of_Generalized_Nets&oldid=3469.
2. Atanassov, K. (1991) *Generalized nets*. Singapore: World Scientific.
3. Atanassov, K. (2007) *On generalized nets theory*. Sofia: Prof. M. Drinov Academic Publishing House.
4. Du, C., Dutta, S., Kurup, P., Yu, T., & Wang, X. (2020) A review of railway infrastructure monitoring using fiber optic sensors. *Sensors and Actuators A: Physical*, 303, 111728. DOI:10.1016/j.sna.2019.111728.
5. Hannan, M.A., Azidin, F. and Azah, M. (2014) Hybrid electric vehicles and their challenges: A review. *Renewable and Sustainable Energy Reviews*, 29, 135–150. DOI:10.1016/j.rser.2013.08.097.
6. Hill, K.O., Fujii, Y., Johnson, D.C. and Kawasaki, B.S. (1978) Photosensitivity in optical fiber waveguides: application to reflection fiber fabrication. *Applied Physics Letters*, 32(10), 647–649. DOI: 10.1063/1.89881.
7. Kashyap, R. (2010) *Fiber bragg gratings*. Academic Press, 2nd edition. DOI:10.1016/C2009-0-16830-7.
8. Kersey, A., Davis, M.A., Patrick, H.J., Leblanc, M., Koo, K., Askins, C.G., Putnam, M. & Friebele, E. (1997) Fiber grating sensors. *Journal of Lightwave Technology*, 15(8), 1442–1463. DOI:10.1109/50.618377.
9. Korbut, M. and Szpica, D. (2021) A review of compressed air engine in the vehicle propulsion system. *Acta Mechanica et Automatica*, 15(4), 215–226. DOI:10.2478/ama-2021-0028.
10. Lemon Liu. (2024) Private technical diagram. T&S Communications Co., Ltd.
11. Linec, M. and Donlagic, D. (2007) A plastic optical fiber microbend sensor used as a low-cost anti-squeeze detector. *IEEE Sensors Journal*, 7(9), 1262–1267. DOI:10.1109/JSEN.2007.901252.
12. Measures, R.M. (2001) *Structural monitoring with fiber optic technology*. San Diego: Academic Press.
13. Othonos, A., & Kalli, K. (1999) *Fiber Bragg gratings: Fundamentals and applications in telecommunications and sensing*. Norwood: Artech House.
14. Peretz, J., Das, S., Tonn, B. (2009) Evaluating knowledge benefits of automotive lightweighting materials R&D projects. *Evaluation and Program Planning*, 32(3), 300-309. DOI:10.1016/j.evalprogplan.2009.03.002.

15. Polishuk, P. (2006) Automotive fiber: Plastic optical fiber builds on MOST success. *Laser Focus World*, 42(3), 57-61.
16. Rao, Y.J. (1999) Recent progress in applications of in-fibre Bragg grating sensors. *Optics and Lasers in Engineering*, 31(4), 297–324. DOI: 10.1016/S0143-8166(99)00025-1.
17. Zarma, T. A., Galadima, A. A. and Maruf, A. A. (2019) Review of motors for electrical vehicles. *Journal of Scientific Research and Reports*, 24(6), 1–6. DOI: 10.9734/jsrr/2019/v24i630170.